Fluid Dynamics
Chapter 11 – Large- and small-scale flows

last edited June 26, 2019
by Olivier Cleynen — https://fluidmech.ninja/

11.1 Motivation

This exploratory chapter is not a critical component of fluid dynamics; instead, it is meant as a brief overview of two extreme cases: flows for which viscous effects are negligible, and flows for which they are dominant. This exploration should allow us to answer two questions:

- How can we model large-scale flows?
- How can we model small-scale flows?

11.2 Flow at large scales

11.2.1 Problem statement

In this section, we are interested in flow at very large scales: those for which a representative length L is very large. In particular, when L is large enough, the influence of viscosity is reduced. Formally, this corresponds to the case where the Reynolds number $[\mathrm{Re}] \equiv \rho V L/\mu$ is very large.

To examine the mechanics of such a flow, we turn to our beloved non-dimensional Navier-Stokes equation for incompressible flow derived as eq. 8/13 p. 164,

$$[\mathrm{St}]\ \frac{\partial \vec{V}^*}{\partial t^*} + [1]\ \vec{V}^* \cdot \vec{\nabla}^* \vec{V}^* = \frac{1}{[\mathrm{Fr}]^2}\ \vec{g}^* - [\mathrm{Eu}]\ \vec{\nabla}^* p^* + \frac{1}{[\mathrm{Re}]}\ \vec{\nabla}^{*2} \vec{V}^* \tag{11/1}$$

We saw in chapter 8 (*Engineering models*) that we could compare the relative weight of terms: when the Reynolds number [Re] is very large, the last term

becomes negligible relative to the other four. Thus, our governing equation can be reduced as follows:

$$[\mathrm{St}]\ \frac{\partial \vec{V}^*}{\partial t^*} + [1]\ \vec{V}^* \cdot \vec{\nabla}^* \vec{V}^* \approx \frac{1}{[\mathrm{Fr}]^2}\ \vec{g}^* - [\mathrm{Eu}]\ \vec{\nabla}^* p^* \tag{11/2}$$

Now, converting eq. 11/2 back to dimensional terms, the governing momentum equation for large-scale flow becomes:

$$\rho \frac{\mathrm{D}\vec{V}}{\mathrm{D}t} = \rho \vec{g} - \vec{\nabla} p \tag{11/3}$$

We see that with the starting proposition that [Re] was large, we have removed altogether the viscous (last) term from the Navier-Stokes equation. Flows governed by this equation are called *inviscid* flows. Equation 11/3 is named the *Euler equation*; it stipulates that the acceleration field is driven only by gravity and by the pressure field.

11.2.2 Investigation of inviscid flows

From what we studied in chapter 8 (*Engineering models*), we recognize immediately that flows governed by eq. 11/3 are troublesome: the absence of viscous effects facilitates the occurrence of turbulence and makes for much more chaotic behaviors. Although the removal of shear from the Navier-Stokes equation simplifies the governing equation, the *solutions* to this new equation become even harder to find and describe.

What can be done in the other two branches of fluid mechanics?

- Large-scale flows are difficult to investigate experimentally. As we have seen in chapter 8 (*Engineering models*), scaling down a flow (e.g. so it may fit inside a laboratory) while maintaining constant [Re] requires increasing velocity by a corresponding factor.
- Large-scale flows are also difficult to investigate numerically. At high [Re], the occurrence of turbulence makes for either an exponential increase in computing power (we saw in chapter 9 that direct numerical simulation computing power increases with $[\mathrm{Re}]^{3,5}$), or for increased reliance on hard-to-calibrate turbulence models (in Reynolds-averaged simulations).

All three branches of fluid mechanics, therefore, struggle with large-scale flows, because of turbulence.

In spite of this, large-scale flows are undeniably important. In chapter 10 we were able to understand and describe fluid flow very close to walls. Now we wish to be able to to the same for large structures, for example, in order to describe the broad patterns of fluid flow (in particular, pressure distribution) in the wake of an aircraft, around a wind turbine, or within a hurricane. It is clear that we have no hope of accounting easily for turbulence, but we can at least describe the main features of such flows by restricting ourselves to laminar cases. In the following sections, we will *model* such laminar solutions directly, based on intuition and observation, and make sure that they match the condition described by eq. 11/3 above.

11.3.1 Kinematics that fit conservation laws

For simple flow structures, the velocity field can be simply described based on observation and intuition. This is done for example in exercise 11.6, where we reconstruct the flow field within and around a tornado using very simple, almost primitive, kinematics.

Without so much as a small increase in complexity, this approach becomes untenable. In the last exercises of chapter 6 (ex. 6.8 & 6.9 p. 133) we have seen that it is easy to propose a velocity field that does not satisfy (is not a solution of) either the mass balance equation or the momentum balance equation. For example, if one considers *two* of the tornado flows mentioned above together, the velocity field cannot be described easily anymore.

One approach has been developed in the 17$^{\text{th}}$ century to overcome this problem. It consists in finding a family of flows, all steady, that *always* satisfy the conservation equations. Those flows can then be added to one another to produce new flows which satisfy the balance equations. Such flows are called *potential flows*.

Two conditions need to be fulfilled for this approach to work:

1. The velocity field must always be describable with a function; that is, there must correspond a single value of u, of v and of w at each of the coordinates x_i, y_i, or z_i in space. This means in practice that we cannot account for flows which "curl up" on themselves, occasionally recirculating back on their path.

2. The velocity field must conserve mass. In incompressible flow, this is achieved if the continuity equation $\vec{\nabla} \cdot \vec{V} = 0$ (eq. 6/35 p. 123) is respected.

With potential flow, these two conditions are addressed as follows:

1. We restrict ourselves to *irrotational* flows, those in which the curl of velocity (see Appendix A3 p. 250) is always null:

$$\vec{\nabla} \times \vec{V} = \vec{0} \tag{11/4}$$

   by definition, for an irrotational flow.

   It can be shown that flows are irrotational when there exists a scalar function ϕ (pronounced "phi" and named *potential function*) of which the gradient is the velocity vector field:

$$\vec{\nabla}\phi \equiv \vec{V} \tag{11/5}$$

   In the case of two-dimensional flow, this translates as:

$$\frac{\partial \phi}{\partial x} \equiv u \tag{11/6}$$

$$\frac{\partial \phi}{\partial y} \equiv v \tag{11/7}$$

   When plotted out, lines of constant ϕ (named *equipotential lines*) are always perpendicular to the streamlines of the flow.

2. The continuity equation is satisfied by referring to stream functions. It can be shown that the divergent of velocity is null when there exists a vector field function $\vec{\psi}$ (pronounced "psi" and named *stream function*) of which the curl is the velocity vector field:

$$\vec{\nabla} \times \vec{\psi} = \vec{V} \tag{11/8}$$

In the case of two-dimensional flow, ψ is a scalar field and eq. 11/8 translates as:

$$\frac{\partial \psi}{\partial y} \equiv u \tag{11/9}$$

$$-\frac{\partial \psi}{\partial x} \equiv v \tag{11/10}$$

When plotted out, lines of of constant ψ value are *streamlines* – in other words, as they travel along, fluid particles follow paths of constant ψ value.

In summary, we have shifted the problem from looking for u and v, to looking for ψ and ϕ. The existence of such functions ensures that flows can be added and subtracted from one another yet will always result in mass-conserving, mathematically-describable flows. If such two functions are known, then the velocity components can be obtained (recovered) easily either in Cartesian coordinates,

$$u = \frac{\partial \phi}{\partial x} = \frac{\partial \psi}{\partial y} \tag{11/11}$$

$$v = \frac{\partial \phi}{\partial y} = -\frac{\partial \psi}{\partial x} \tag{11/12}$$

or angular coordinates:

$$v_r = \frac{\partial \phi}{\partial r} = \frac{1}{r}\frac{\partial \psi}{\partial \theta} \tag{11/13}$$

$$v_\theta = \frac{1}{r}\frac{\partial \phi}{\partial \theta} = -\frac{\partial \psi}{\partial r} \tag{11/14}$$

11.3.2 Strengths and weaknesses of potential flow

The potential flow methodology allows us to find solutions to the Euler equation: flows in which the Reynolds number is high enough that viscosity has no significant role anymore. Potential flows are the simplest solutions that we are able to come up with. They are:

- strictly steady;
- inviscid;
- incompressible;
- devoid of energy transfers;
- two-dimensional (in the scope of this course at least).

This is quite convenient for the academician, who recognizes immediately four of the five criteria which we set forth in chapter 2 (*Analysis of existing*

flows with one dimension) for using the Bernoulli equation. Along a streamline, the fifth condition is met, and Euler's equation reduces to eq. 2/20 (p. 42), reproduced here:

$$\frac{p_1}{\rho} + \frac{1}{2}V_1^2 + gz_1 = \frac{p_2}{\rho} + \frac{1}{2}V_2^2 + gz_2 = \text{cst.} \tag{11/15}$$

along a streamline in a steady incompressible inviscid flow.

and so it follows that if the solution to a potential flow is known, the pressure is known everywhere, and the forces due to pressure can be calculated with relative ease.

Nevertheless, from a science and engineering point of view, potential flows have only limited value, because they are entirely unable to account for turbulence, which we have seen is an integral feature of high-[Re] flows. We should therefore use them only with great caution. Potential flows help us model large-scale structures with very little computational cost, but this comes with strong limitations.

11.3.3 Superposition: the lifting cylinder

It is possible to describe a handful of basic potential flows called *elementary flows* as fundamental ingredients that can be added to one another to create more complex and interesting flows. Without going into much detail, the most relevant elementary flows are:

- Uniform longitudinal flow,

$$\phi = V\, r \cos\theta \tag{11/16}$$
$$\psi = V\, r \sin\theta \tag{11/17}$$

- *Sources* and *sinks* (fig. 11.1) which are associated with the appearance of a (positive or negative) volume flow rate $\dot{\mathcal{V}}$ from a single point in the flow:

$$\phi = \frac{\dot{\mathcal{V}}}{2\pi} \ln r \tag{11/18}$$
$$\psi = \frac{\dot{\mathcal{V}}}{2\pi}\theta \tag{11/19}$$

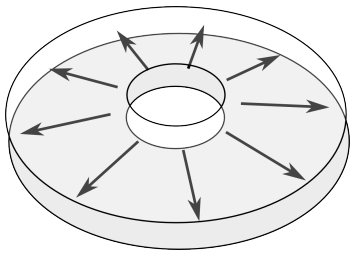

Figure 11.1: Concept of a source inside a two-dimensional potential flow. A sink would display exactly opposed velocities.

Figure CC-BY-SA *Commons User:Nicoguaro*

- *Irrotational vortices*, rotational patterns which impart a rotational velocity $v_\theta = f(r, \theta)$ on the flow, in addition to which there may exist a radial component v_r:

$$\phi = \frac{\Gamma}{2\pi}\theta \tag{11/20}$$

$$\psi = -\frac{\Gamma}{2\pi}\ln r \tag{11/21}$$

  in which Γ (termed *circulation*) is a constant proportional to the strength of the vortex.

- *Doublets*, which consist in a source and a sink of equal volume flow rate positioned extremely close one to another (fig. 11.2):

$$\phi = K\frac{\cos\theta}{r} \tag{11/22}$$

$$\psi = -K\frac{\sin\theta}{r} \tag{11/23}$$

  in which K is a constant proportional to the source/sink volume flow rate $\dot{\mathcal{V}}$.

It was found in the 17th Century that combining a doublet with uniform flow resulted in flow patterns that imiated "perfect" flow around a cylinder: a flow where the fluid flows smoothly and steadily everywhere (fig. 11.3). The stream function of that flow is:

$$\psi = U_\infty \sin\theta\left(r - \frac{R^2}{r}\right) \tag{11/24}$$

This stream function allows us to describe the velocity everywhere:

$$v_r = \frac{1}{r}\frac{\partial\psi}{\partial\theta} = U_\infty\cos\theta\left(1 - \frac{R^2}{r^2}\right) \tag{11/25}$$

$$v_\theta = -\frac{\partial\psi}{\partial r} = -U_\infty\sin\theta\left(1 + \frac{R^2}{r^2}\right) \tag{11/26}$$

We can even calculate the lift and drag applying on the cylinder surface. Indeed, along the cylinder wall, $r = R$ and

$$v_r|_{r=R} = 0 \tag{11/27}$$

$$v_\theta|_{r=R} = -2U_\infty\sin\theta \tag{11/28}$$

Since the Bernoulli equation can be applied along any streamline in this (steady, constant-energy, inviscid, incompressible) flow, we can express the

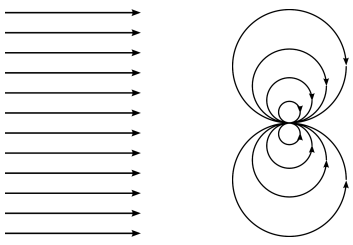

Figure 11.2: Left: a simple uniform steady flow; Right: a *doublet*, the result of a source and a sink brought very close one to another

Figure CC-0 *Olivier Cleynen*

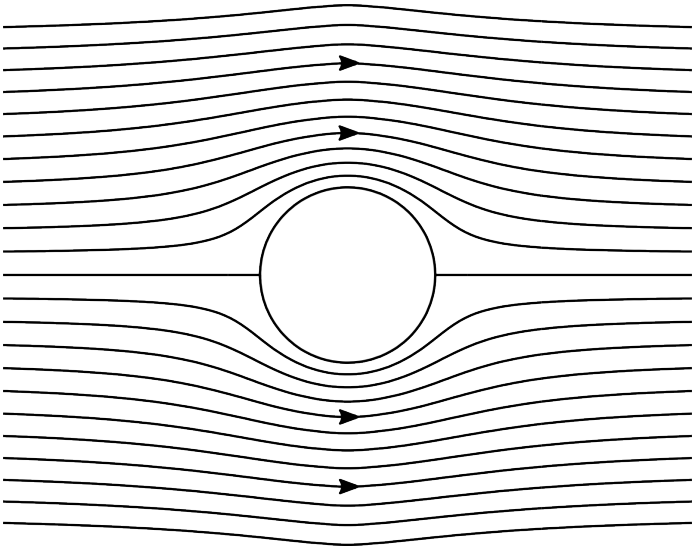

Figure 11.3: The addition of a *doublet* and a *uniform flow* produces streamlines for an (idealized) flow around a cylinder.

Figure CC-BY-SA *by Commons User:Kraaiennest*

pressure p_s on the cylinder surface as a function of θ:

$$p_\infty + \frac{1}{2}\rho U_\infty^2 = p_s + \frac{1}{2}\rho v_\theta^2$$

$$p_{s\,(\theta)} = p_\infty + \frac{1}{2}\rho\left(U_\infty^2 - v_\theta^2\right) \tag{11/29}$$

Now, a relatively simple integration gives us the net forces exerted by the fluid on the cylinder per unit width L, in each of the two directions x and y:

$$\frac{F_{\text{net},x}}{L} = -\int_0^{2\pi} p_s \cos\theta \, R \, \mathrm{d}\theta = 0 \tag{11/30}$$

$$\frac{F_{\text{net},y}}{L} = -\int_0^{2\pi} p_s \sin\theta \, R \, \mathrm{d}\theta = 0 \tag{11/31}$$

The results are interesting, and at the time they were obtained by their author, Jean le Rond D'Alembert, were devastating: both lift and drag are zero. This inability to reproduce the well-known phenomena of drag is often called the *d'Alembert paradox*.

To find out why the solution is not realistic, we can plot the resulting surce pressure distribution graphically, and compared to experimental measurements: this is done in fig. 11.4. Good agreement is obtained on the leading edge of the cylinder; but as the pressure gradient becomes unfavorable, in practice the boundary layer separates –a phenomenon that *cannot* be described with inviscid flow— and a low-pressure area forms on the downstream side of the cylinder.

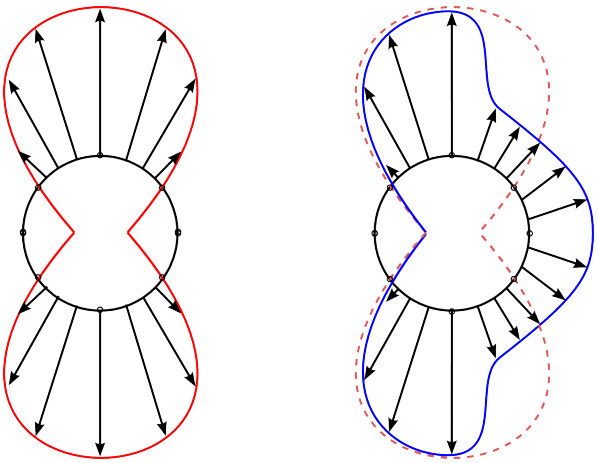

Figure 11.4: Pressure distribution (relative to the far-flow pressure) on the surface of a cylinder, with flow from left to right. On the left is the potential flow case, purely symmetrical. On the right (in blue) is a measurement made at a high Reynolds number. Boundary layer separation occurs on the second half of the cylinder, which prevents the recovery of leading-edge pressure values, and increases drag.

Figure CC-BY-SA *Commons User:BoH & Olivier Cleynen*

11.3.4 Circulating cylinder

Video: watch the Brazilian football team show their French counterparts how circulation (induced through friction by ball rotation) is associated to dynamic lift on a circular body

by TF1, 1997 (STYL)
https://youtu.be/oGeMZ3t8jn4

An extremely interesting "hack" can be implemented with the potential cylinder flow above if an irrotational vortex of stream function $\psi = -\frac{\Gamma}{2\pi}\ln r$ (eq. 11/21) is added to it. The overall flow field becomes:

$$\psi = U_\infty \sin\theta \left(r - \frac{R^2}{r} \right) - \frac{\Gamma}{2\pi}\ln r \tag{11/32}$$

With this function, several key characteristics of the flow field can be obtained. The first is the velocity field at the cylinder surface:

$$v_r|_{r=R} = 0 \tag{11/33}$$

$$v_\theta|_{r=R} = -2U_\infty \sin\theta + \frac{\Gamma}{2\pi R} \tag{11/34}$$

and we immediately notice that the velocity distribution is no longer symmetrical with respect to the horizontal axis (fig. 11.5): the fluid is deflected, and so there will be a net force on the cylinder.

This time, the net pressure forces on the cylinder have changed:

$$\frac{F_{\text{net},x}}{L} = -\int_0^{2\pi} p_s \cos\theta \, R \, \mathrm{d}\theta = 0 \tag{11/35}$$

$$\frac{F_{\text{net},y}}{L} = -\int_0^{2\pi} p_s \sin\theta \, R \, \mathrm{d}\theta = -\rho \, U_\infty \, \Gamma \tag{11/36}$$

We thus find out that **the drag is once again zero** —as for any potential flow— but that **lift occurs** which is proportional to the free-stream velocity U and to the circulation Γ.

In practice, such a flow can be generated by spinning a cylindrical object in a uniform flow. A lateral force is then obtained, which can be used as a propulsive or sustaining force. Several boats and even an aircraft have been used in practice to demonstrate this principle. Naturally, flow separation from the cylinder profile and the high shear efforts generated on the surface

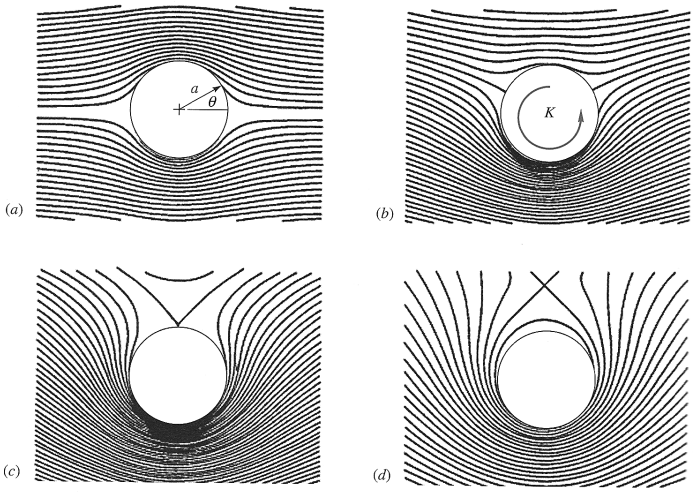

Figure 11.5: The addition of an irrotational vortex on top of the cylinder flow described in fig. 11.3 distorts the flow field and it becomes asymmetrical: a lift force is developed, which depends directly on the circulation Γ.

Figure © White 2008 [22]

cause real flows to differ from the ideal case described here, and it turns out that rotating cylinders are a horribly uneconomical and unpractical way of generating lift.

11.3.5 Modeling lift with circulation

Video: acting on swimming pool water with a round plate sheds a half-circular vortex that is extremely stable and can be interacted with quite easily. Such stable laminar structures are excellent candidates for analysis using potential flow.
by Physics Girl (Dianna Cowern) (STYL)
https://youtu.be/pnbJEg9r1o8

Fluid flow around cylinders may have little appeal for the modern student of fluid mechanics, but the methodology above has been taken much further. With further mathematical manipulation called *conformal mapping*, potential flow can be used to described flow around geometrical shapes such as airfoils (fig. 11.6). Because the flow around such streamlined bodies usually does not feature boundary layer separation, the predicted flow fields everywhere except in the close vicinity of the solid surface are accurately predicted.

There again, it is observed that regardless of the constructed geometry, no lift can be modeled unless circulation is also added within the flow. The amount of circulation needed so that results may correspond to experimental observations is found by increasing it progressively until the the rear stagnation point reaches the rear trailing edge of the airfoil, a condition known as the *Kutta condition*. Regardless of the amount of circulation added, potential flow remains entirely reversible, both in a kinematic and a thermodynamic sense, thus, care must be taken in the problem setup to make sure the model is realistic (fig. 11.7).

It is then observed in general that *any* dynamic lift generation can be modeled as the superposition of a free-stream flow and a circulation effect (fig. 11.8). With such a tool, potential flow becomes an extremely useful tool, mathematically and computationally inexpensive, in order to model and understand the cause and effect of dynamic lift in fluid mechanics. In particular, it has been paramount in the description of aerodynamic lift distribution over aircraft wing surfaces (fig. 11.9), with a concept called the Lifting-line theory.

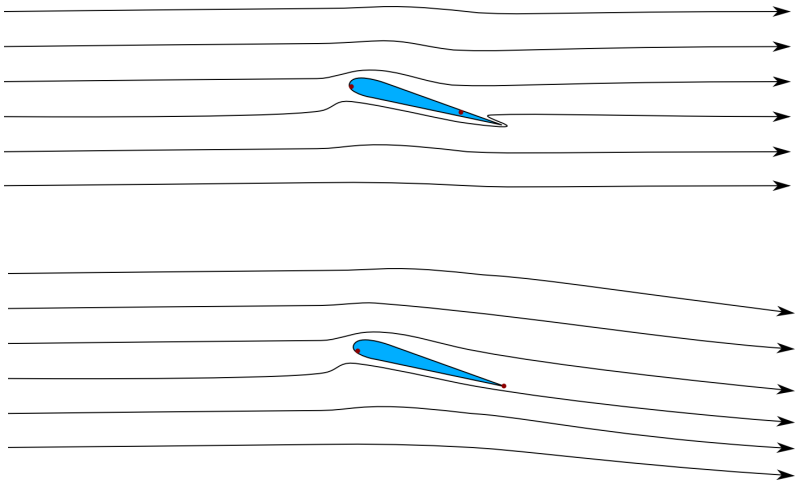

Figure 11.6: Potential flow around an airfoil without (top) and with (bottom) circulation. Much like potential flow around a cylinder, potential flow around an airfoil can only result in a net vertical force if an irrotational vortex (with circulation Γ) is added on top of the flow. Only one value for Γ will generate a realistic flow, with the rear stagnation point coinciding with the trailing edge, a occurrence named *Kutta condition*.

Figure CC-0 *Olivier Cleynen*

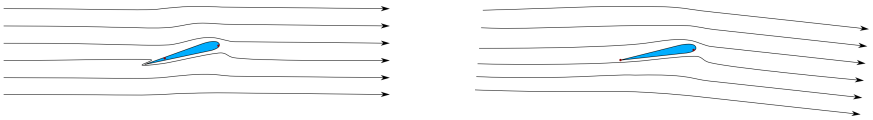

Figure 11.7: Potential flow allows all velocities to be inverted without any change in the flow geometry. Here the flow around an airfoil is reversed, displaying unphysical behavior.

Figure CC-0 *Olivier Cleynen*

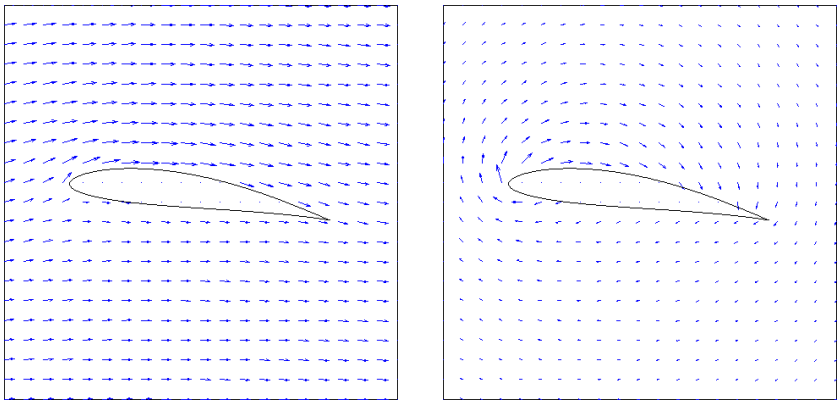

Figure 11.8: A numerical model of flow around an airfoil. In the left figure, the velocity vectors are represented relative to a stationary background. In the right figure, the velocity of the free-stream flow has been subtracted from each vector, bringing the circulation phenomenon into evidence.

Figures 1 & 2 CC-BY-SA *by en:Wikipedia User:Crowsnest*

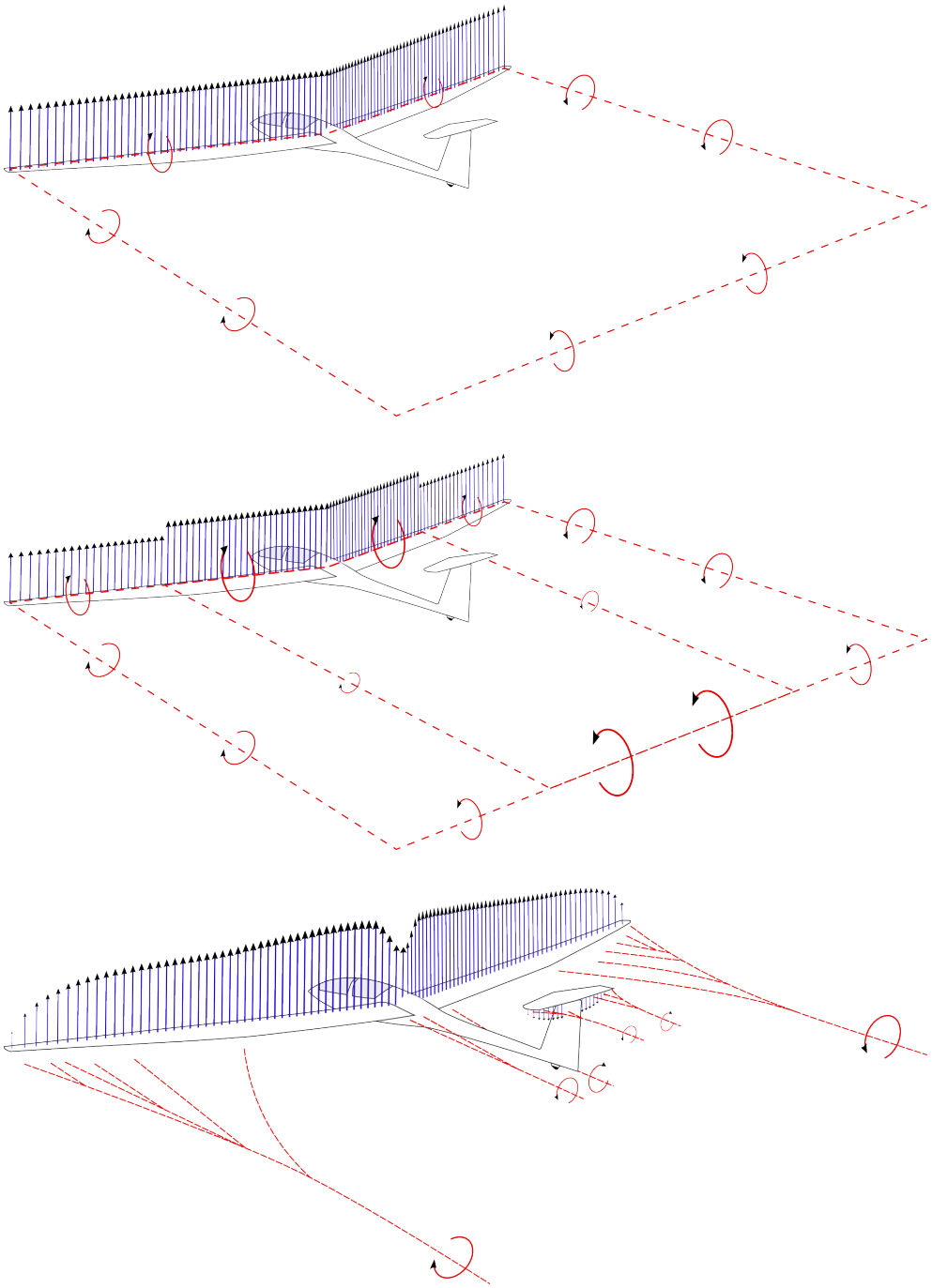

Figure 11.9: From top to bottom, the lift distribution over the wings of a glider is modeled with increasingly complex (and accurate) lift and circulation distributions along the span. The Lifting-line theory is a method associating each element of lift with a certain amount of circulation. The effect of each span-wise change of circulation is then mapped onto the flow field as a trailing vortex.

11.4 Flow at very small scales

At the complete opposite of the spectrum, we find flow at very small scales: flows around bacteria, dust particles, and inside very small ducts. In those flows the representative length L is extremely small, which makes for small values of the Reynolds number. Such flows are termed *creeping* or *Stokes flows*. What are their main characteristics?

Looking back once again at the non-dimensional Navier-Stokes equation for incompressible flow derived as eq. 8/13 p. 164,

$$[\mathrm{St}]\,\frac{\partial \vec{V}^*}{\partial t^*} + [1]\,\vec{V}^* \cdot \vec{\nabla}^* \vec{V}^* = \frac{1}{[\mathrm{Fr}]^2}\,\vec{g}^* - [\mathrm{Eu}]\,\vec{\nabla}^* p^* + \frac{1}{[\mathrm{Re}]}\,\vec{\nabla}^{*2}\vec{V}^* \qquad (11/37)$$

we see that creeping flow will occur when the Reynolds number is much smaller than 1. The relative weight of the term $(1/[\mathrm{Re}])\,\vec{\nabla}^{*2}\vec{V}^*$ then becomes overwhelming.

In addition to cases where $[\mathrm{Re}] \ll 1$, we focus our interest on flows for which:

- gravitational effects have negligible influence over the velocity field;
- the characteristic frequency is extremely low (quasi-steady flow).

With these characteristics, the terms associated with the [St] (Strouhal) and [Fr] (Froude) numbers become very small with respect to the other terms, and our non-dimensionalized Navier-Stokes equation (eq. 11/37) is approximately reduced to:

$$\vec{0} \approx -[\mathrm{Eu}]\,\vec{\nabla}^* p^* + \frac{1}{[\mathrm{Re}]}\,\vec{\nabla}^{*2}\vec{V}^* \qquad (11/38)$$

We can now come back to dimensionalized equations, concluding that for a fluid flow dominated by viscosity, the pressure and velocity fields are linked together by the approximate relation:

$$\vec{\nabla} p = \mu \vec{\nabla}^2 \vec{V} \qquad (11/39)$$

In this type of flow, the pressure field is entirely dictated by the Laplacian of velocity, and the fluid density has no importance. Micro-organisms, for which the representative length L is very small, spend their lives in such flows (fig. 11.10). At the human scale, we can visualize the effects of these flows by moving an object slowly in highly-viscous fluids (e.g. a spoon in honey), or by swimming in a pool filled with plastic balls. The inertial effects are almost inexistent, drag is extremely important, and the object geometry has comparatively small influence.

In 1851, George Gabriel Stokes worked through equation 11/39 for flow around a sphere, and obtained an analytical solution for the flow field. This allowed him to show that the drag $F_{\mathrm{D\ sphere}}$ applying on a sphere of diameter D in creeping flow (fig. 11.11) is:

$$F_{\mathrm{D\ sphere}} = 3\pi\mu U_\infty D \qquad (11/40)$$

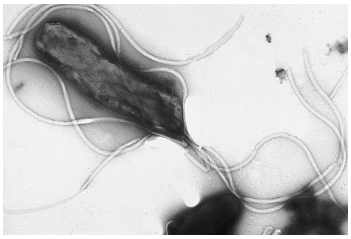

Figure 11.10: Micro-organisms carry themselves through fluids at extremely low Reynolds numbers, since their scale L is very small. For them, viscosity effects dominate inertial effects.

Photo by Yutaka Tsutsumi, M.D., Fujita Health University School of Medicine

Inserting this equation 11/40 into the definition of the drag coefficient $C_{FD} \equiv F_D/\frac{1}{2}\rho S_{\text{frontal}} U_\infty^2$ (from eq. 8/15 p. 169) then yields:

$$C_{FD} = \frac{F_{\text{D sphere}}}{\frac{1}{2}\rho U_\infty^2 \frac{\pi}{4} D^2} = \frac{24\mu}{\rho\, U_\infty D} = \frac{24}{[\text{Re}]_D} \tag{11/41}$$

These equations are specific to flow around spheres, but the trends they describe apply well to most bodies evolving in highly-viscous flows, such as dust or liquid particles traveling through the atmosphere. Drag is only proportional to the speed (as opposed to low-viscosity flows in which it grows with velocity *squared*), and it does not depend on fluid density.

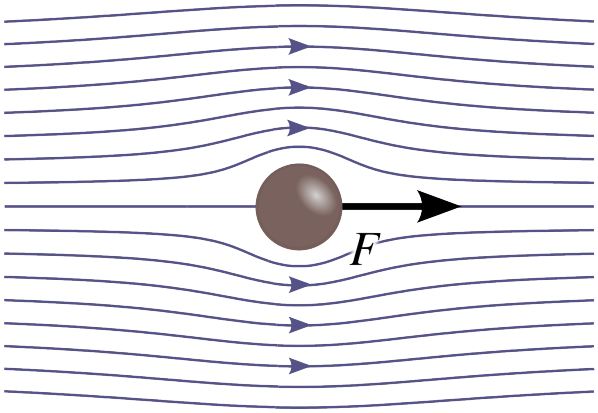

Figure 11.11: Flow at very low Reynolds numbers around a sphere. In this regime, the drag force is proportional to the velocity.

Figure CC-BY-SA *by Olivier Cleynen & Commons User:Kraaiennest*

Problem sheet 11: Large- and small-scale flows

last edited June 26, 2019
by Olivier Cleynen — https://fluidmech.ninja/

These notes are based on textbooks by White [22], Çengel & al.[25], Munson & al.[29], and de Nevers [17].

Except otherwise indicated, assume that:
The atmosphere has $p_{\text{atm.}} = 1\,\text{bar}$; $\rho_{\text{atm.}} = 1{,}225\,\text{kg m}^{-3}$; $T_{\text{atm.}} = 11{,}3\,^{\circ}\text{C}$; $\mu_{\text{atm.}} = 1{,}5 \cdot 10^{-5}\,\text{Pa s}$
Air behaves as a perfect gas: R_{air}=287 $\text{J kg}^{-1}\,\text{K}^{-1}$; γ_{air}=1,4; $c_{p\,\text{air}}$=1 005 $\text{J kg}^{-1}\,\text{K}^{-1}$; $c_{v\,\text{air}}$=718 $\text{J kg}^{-1}\,\text{K}^{-1}$
Liquid water is incompressible: $\rho_{\text{water}} = 1\,000\,\text{kg m}^{-3}$, $c_{p\,\text{water}} = 4\,180\,\text{J kg}^{-1}\,\text{K}^{-1}$

In a highly-viscous (creeping) steady flow, the drag F_{D} exerted on a spherical body of diameter D at by flow at velocity U_∞ is quantified as:

$$F_{\text{D sphere}} = 3\pi\mu U_\infty D \tag{11/40}$$

11.1 Volcanic ash from the Eyjafjallajökull

Çengel & al. [25] E10.2

In 2010, a volcano with a complicated name and unpredictable mood decided to ground the entire European airline industry for five days.

We consider a microscopic ash particle released at very high altitude (−50 °C, 0,55 bar, $1{,}474 \cdot 10^{-5}\,\text{N s m}^{-2}$). We model it as a sphere with 50 µm diameter. The density of volcanic ash is $1\,240\,\text{kg m}^{-3}$.

11.1.1. What is the terminal velocity of the particle?

11.1.2. Will this terminal velocity increase or decrease as the particle progresses towards the ground? (briefly justify your answer, e.g. in 30 words or less)

11.2 Water drop

Çengel & al. [25] 10-21

A rainy day provides yet another opportunity for exploring fluid dynamics (fig. 11.12). A water drop with diameter 42,4 µm is falling through air at 25 °C and 1 bar.

11.2.1. Which terminal velocity will it reach?

11.2.2. Which velocity will it reach once its diameter will have doubled?

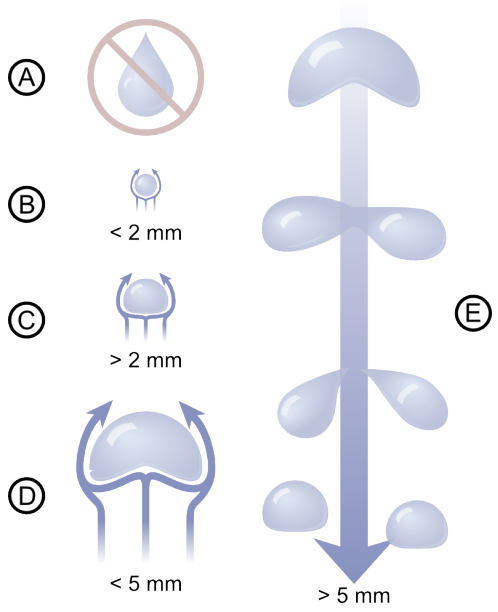

Figure 11.12: A sketched diagram showing the geometry of water drops of various sizes in free fall. When their diameter is lower than 2 mm, water drops are approximately spherical (B). As they grow beyond this size, their shape changes and they eventually break-up (C-E). They never display the "classical" shape displayed in A, which is caused only by surface tension effects when they drip from solid surfaces.

Figure CC-BY-SA *by Ryan Wilson*

11.3 Idealized flow over a hangar roof

based on White [22] P8.54

Certain flows in which both compressibility and viscosity effects are negligible can be described using the potential flow assumption (the hypothesis that the flow is everywhere irrotational). If we compute the two-dimensional laminar steady fluid flow around a cylinder profile, we obtain the velocities in polar coordinates as:

$$v_r = V_\infty \cos\theta \left(1 - \frac{R^2}{r^2}\right) \tag{11/25}$$

$$v_\theta = -V_\infty \sin\theta \left(1 + \frac{R^2}{r^2}\right) \tag{11/26}$$

where the origin ($r = 0$) is at the center of the cylinder profile;
θ is measured relative to the free-stream velocity vector;
V_∞ is the incoming free-stream velocity;
and R is the (fixed) cylinder radius.

In this exercise, we study the air flow over a hangar roof with this model. We use the equations above to describe the air velocity everywhere, pretending the as the wind blows about a large semi-cylindrical solid structure — an idealized description of an otherwise complex flow.

Wind with a nearly-uniform velocity $U_\infty = 100\,\mathrm{km\,h^{-1}}$ is blowing across a 50 m-long hangar with a semi-cylindrical geometry, as shown in fig. 11.13. The radius of the hangar is $R = 20\,\mathrm{m}$.

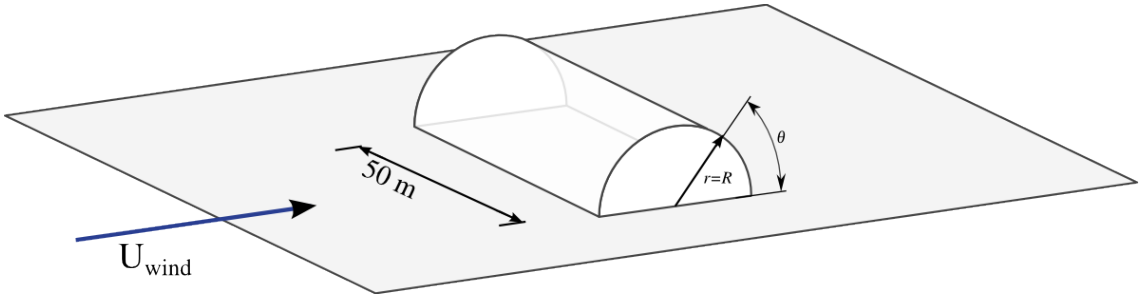

Figure 11.13: A semi-cylindrical hangar roof. Wind with uniform velocity U flows perpendicular to the cylinder axis.

Figure CC-0 *Olivier Cleynen*

11.3.1. Starting from eqs. 11/25 and 11/26, show that the pressure p_s on the surface on the roof is distributed as:

$$p_s = p_\infty + \frac{1}{2}\rho\left(V_\infty^2 - 4V_\infty^2 \sin^2\theta\right) \tag{11/42}$$

11.3.2. The pressure inside the hangar is set to p_∞. What is the total lift force on the hangar?
(see also problem 4.6 p. 87)
(a couple of hints to help with the algebra: $\int \sin x \,\mathrm{d}x = -\cos x + k$ and $\int \sin^3 x \,\mathrm{d}x = \frac{1}{3}\cos^3 x - \cos x + k$).

11.3.3. At which position on the roof is the $p_s = p_\infty$?

11.3.4. Describe briefly (e.g. in 30 words or less) two reasons why the results above would not correspond to reality.

11.4 Cabling of the Wright Flyer

derived from Munson & al. [29] 9.106

The *Wright Flyer I*, the first powered and controlled aircraft in history, was subjected to multiple types of drag. We have already studied viscous friction on its thin wings in exercise 7.4. The data in figure 11.14 provides the opportunity to quantify drag due to pressure.

A network of metal cables with diameter 1,27 mm criss-crossed the aircraft in order to provide structural rigidity. The cables were positioned perpendicularly to the air flow, which came at 40 $\mathrm{km\,h^{-1}}$. The total cable length was approximately 60 m.

What was the drag generated by the cables?

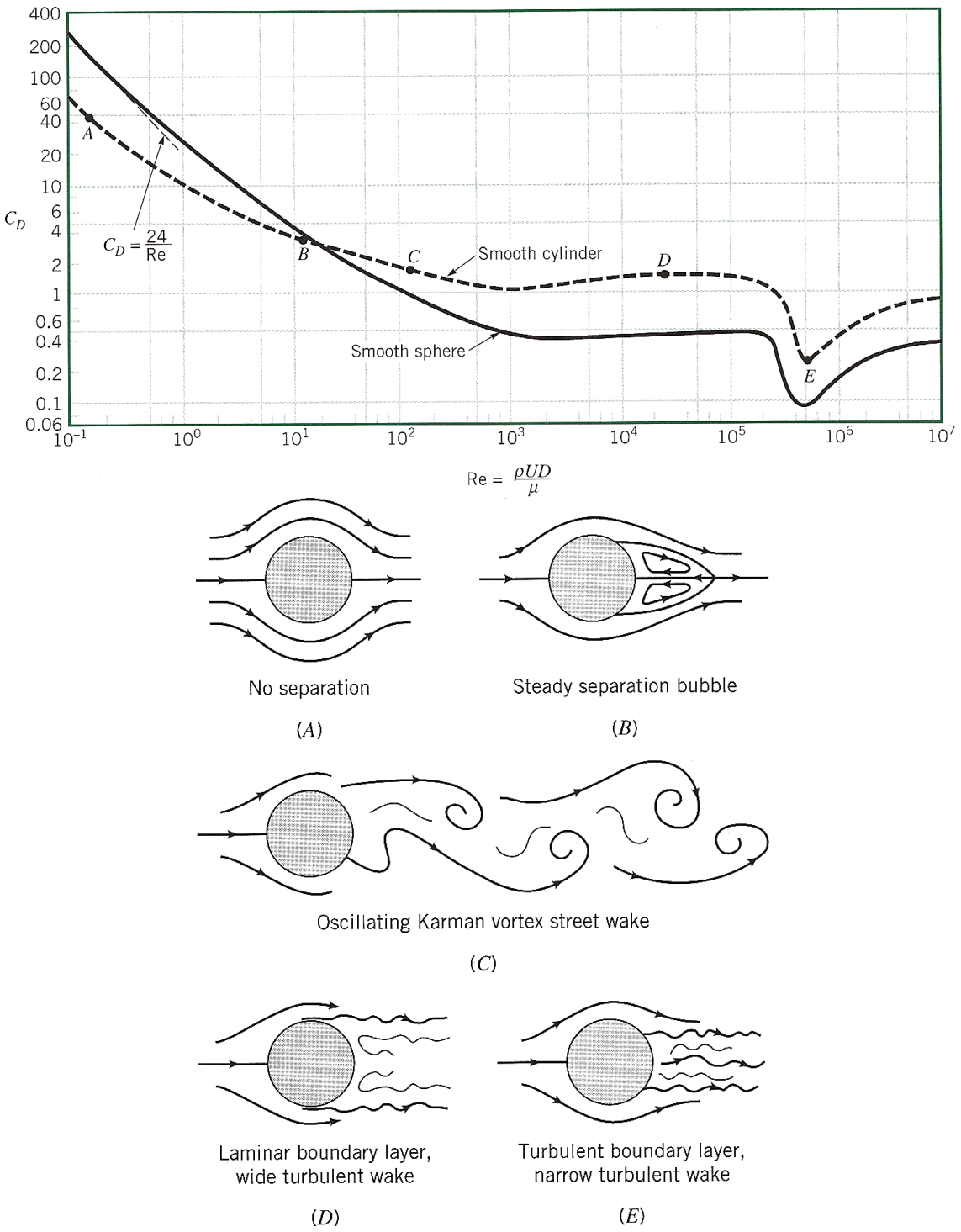

Figure 11.14: Experimental measurements of the drag coefficient applying to a cylinder and to a sphere as a function of the diameter-based Reynolds number $[\mathrm{Re}]_D$, shown together with schematic depictions of the flow around the cylinder. By convention, the *drag coefficient* $C_\mathrm{D} \equiv C_{F\,\mathrm{D}} \equiv \frac{F_\mathrm{D}}{\frac{1}{2}\rho S U_\infty^2}$ (eq. 8/15 p. 169) compares the drag force F_D with the frontal area S.

Both figures © from Munson & al.[29]

11.5 Ping pong ball

Munson & al. [29] E9.16

A series of experiments is conducted in a wind tunnel on a large cast iron ball with a smooth surface; the results are shown in fig. 11.15. These measurement data are used to predict the behavior of a ping pong ball. Table tennis regulations constrain the mass of the ball to 2,7 g and its diameter to 40 mm.

11.5.1. Is it possible for a ball thrown at a speed of $50\,\mathrm{km\,h^{-1}}$ to have a perfectly horizontal trajectory?

11.5.2. If so, what would be its deceleration?

11.5.3. How would the drag and lift applying on the ball evolve if the air viscosity was progressively decreased to zero?

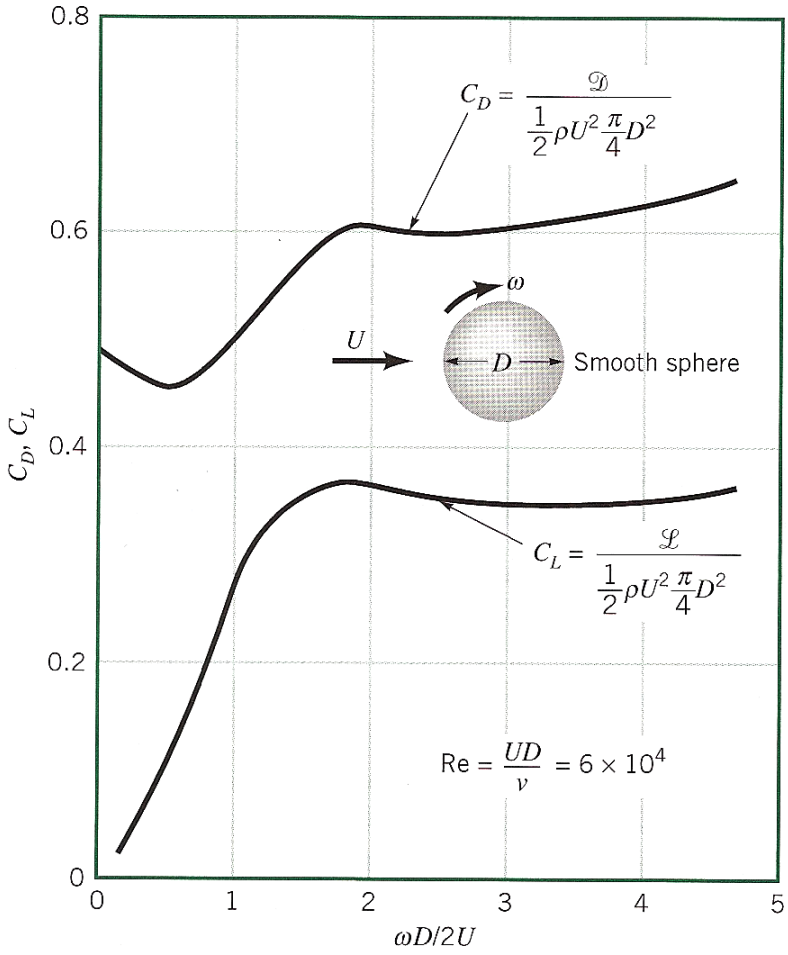

Figure 11.15: Experimental measurements of the lift and drag coefficients applying on a rotating sphere in an steady uniform flow.

Figure © from Munson & al.[29]

11.6 Flow field of a tornado

Çengel & al. [25] E9-5, E9-14 & E10-3

In this problem, we attempt to model a very large-scale flow: that of a tornado (fig. 11.16). We begin by pretending the tornado is one perfectly straight, stationary structure. We divide the flow into two regions: a core cylinder that rotates almost like a solid body, and an outer region where flow spins in an irrotational matter. This model is called the Rankine vortex (displayed in fig. 11.17) and is used widely as a simple, first approximation to model flows as large as a hurricane and as small as turbulence-induced vortices.

Figure 11.16: Photo of an approaching tornado in Manitoba, Canada

Photo CC-BY-SA *by Commons User:Grhu*

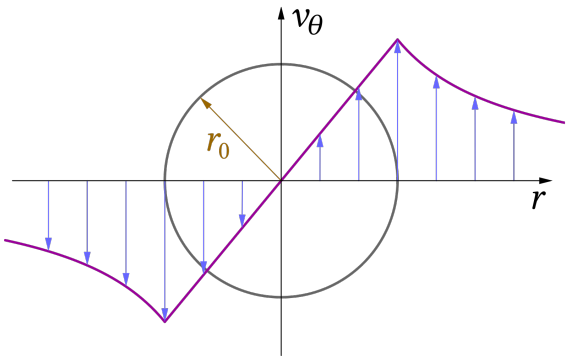

Figure 11.17: Modeled angular velocity in a vortex, according to the Rankine vortex model

Figure CC-BY-SA *by en:Wikipedia User:Justin1569*

We are first interested in the outer region of the tornado flow field. We model the flow as being steady, two-dimensional (neglecting any movement in the vertical, z-direction), and having a rotational velocity v_θ such that:

$$v_\theta = \frac{\Gamma}{2\pi r} \tag{11/43}$$

in which Γ is the *circulation* (measured in s^{-1}) and remains constant and uniform.

11.6.1. The mass balance equation for incompressible flow (eq. 6/35 p. 123) is developed in cylindrical coordinates as follows:

$$\frac{1}{r}\frac{\partial r v_r}{\partial r} + \frac{1}{r}\frac{\partial v_\theta}{\partial \theta} + \frac{\partial v_z}{\partial z} = 0 \tag{11/44}$$

According to this mass balance equation, what form must the radial velocity v_r take?

Among all the possibilities for v_r, we choose the simplest form, so that from now on, we model radial velocity as:

$$v_r = 0 \tag{11/45}$$

11.6.2. The momentum balance equation for incompressible flow (eq. 6/42 p. 125) is developed in cylindrical coordinates are as follows:

$$\rho\left[\frac{\partial v_r}{\partial t} + v_r\frac{\partial v_r}{\partial r} + \frac{v_\theta}{r}\frac{\partial v_r}{\partial \theta} - \frac{v_\theta^2}{r} + v_z\frac{\partial v_r}{\partial z}\right] = \rho g_r - \frac{\partial p}{\partial r} + \mu\left[\frac{1}{r}\frac{\partial}{\partial r}\left(r\frac{\partial v_r}{\partial r}\right) - \frac{v_r}{r^2} + \frac{1}{r^2}\frac{\partial^2 v_r}{(\partial\theta)^2} - \frac{2}{r^2}\frac{\partial v_\theta}{\partial\theta} + \frac{\partial^2 v_r}{(\partial z)^2}\right] \tag{11/46}$$

$$\rho\left[\frac{\partial v_\theta}{\partial t} + v_r\frac{\partial v_\theta}{\partial r} + \frac{v_\theta}{r}\frac{\partial v_\theta}{\partial \theta} + \frac{v_r v_\theta}{r} + v_z\frac{\partial v_\theta}{\partial z}\right] = \rho g_\theta - \frac{1}{r}\frac{\partial p}{\partial \theta} + \mu\left[\frac{1}{r}\frac{\partial}{\partial r}\left(r\frac{\partial v_\theta}{\partial r}\right) - \frac{v_\theta}{r^2} + \frac{1}{r^2}\frac{\partial^2 v_\theta}{(\partial\theta)^2} + \frac{2}{r^2}\frac{\partial v_r}{\partial\theta} + \frac{\partial^2 v_\theta}{(\partial z)^2}\right] \tag{11/47}$$

$$\rho\left[\frac{\partial v_z}{\partial t} + v_r\frac{\partial v_z}{\partial r} + \frac{v_\theta}{r}\frac{\partial v_r}{\partial \theta} + v_z\frac{\partial v_z}{\partial z}\right] = \rho g_z - \frac{\partial p}{\partial z} + \mu\left[\frac{1}{r}\frac{\partial}{\partial r}\left(r\frac{\partial v_z}{\partial r}\right) + \frac{1}{r^2}\frac{\partial^2 v_z}{(\partial\theta)^2} + \frac{\partial^2 v_z}{(\partial z)^2}\right] \tag{11/48}$$

Starting from those equations, show that the pressure distribution in the outer region of the tornado can be expressed as:

$$p = p_\infty - \frac{1}{2}\rho\,\Gamma^2\frac{1}{r^2} \tag{11/49}$$

where p_∞ is the atmospheric pressure far away from the tornado.

We now turn to the core of the tornado, which we model as if it were a rotating solid (a *vortex core*).

11.6.3. What is the radial velocity v_θ distribution?

11.6.4. What is the pressure field within the rotational core of the tornado?
(hint: you may start directly from an energy balance equation, eq. 2/18 p. 40, without having to use the Navier-Stokes equations above).

11.6.5. Make a simple, qualitative sketch (i.e. without numerical data) of the pressure as a function of radius throughout the entire tornado flow field.

It is finally time to calibrate and exploit our model. We estimate the tornado diameter to be 50 m and the maximum wind velocity to be 180 $\mathrm{km\,h^{-1}}$.

11.6.6. According to the model, what is the lowest pressure attained by the air?

11.6.7. According to the model, at what distance from the core are winds lower than 50 $\mathrm{km\,h^{-1}}$?

(curious students may play with the above model by adding a non-zero radial velocity, and look up the phenomenon of *vortex stretching*)

11.7 Lift on a symmetrical object

non-examinable

Briefly explain (e.g. with answers 30 words or less) how lift can be generated on a sphere or a cylinder,

- with differential control boundary layer control;
- with the effect of rotation.

Draw a few streamlines in a two-dimensional sketch of the phenomenon.

11.8 Air flow over a wing profile

From Munson & al. [29] 9.109

The characteristics of a thin, flat-bottomed airfoil are examined by a group of students in a wind tunnel. The first investigations focus on the boundary layer, and the research group evaluate the boundary layer thickness and make sure that it is fully attached.

Once this is done, the group proceeds with speed measurements all around the airfoil. Measurements of the longitudinal speed u just above the boundary layer on the top surface are tabulated below:

x/c (%)	y/c (%)	u/U
0	0	0
2,5	3,72	0,971
5	5,3	1,232
7,5	6,48	1,273
10	7,43	1,271
20	9,92	1,276
30	11,14	1,295
40	10,49	1,307
50	10,45	1,308
60	9,11	1,195
70	6,46	1,065
80	3,62	0,945
90	1,26	0,856
100	0	0,807

On the bottom surface, the speed is measured as being constant ($u = U$) to within experimental error.

What is the lift coefficient of the airfoil?

Answers

11.1 1) At terminal velocity, the weight of the sphere equals the drag. This allows us to obtain $U = g\rho_{\text{sphere}}\frac{D^2}{18\mu} = 0{,}1146\,\text{m s}^{-1}$: unbearably slow when you are stuck in an airport! With U, check that the Reynolds number indeed corresponds to creeping flow: $[\text{Re}]_D = 0{,}334$.

11.2 Same as previous exercise: $U_1 = 4{,}578 \cdot 10^{-2}\,\text{m s}^{-1}$ and $U_2 = 0{,}183\,\text{m s}^{-1}$, with Reynolds numbers of 0,113 and 0,906 respectively (thus creeping flow hypothesis valid).

11.3 1) Integrate the vertical component of force due to pressure: $F_{\text{L roof}} = 1{,}575\,\text{MN}$.

11.4 A simple reading of fig. 11.14 gives $F_{\text{D}} = 6{,}9\,\text{N}$, $\dot{W} = 76\,\text{W}$.

11.5 Yes — a reading of fig. 11.13 gives $\omega = 83\,\text{rev/s}$.